

SIGMAE: A Spectral-Index-Guided Foundation Model for Multispectral Remote Sensing

Xiaokang Zhang^a, Bo Li^b, Chufeng Zhou^c, Weikang Yu^d and Lefei Zhang^e

^aSchool of Artificial Intelligence, Wuhan University, Wuhan, 430072, China

^bSchool of Artificial Intelligence and Automation, Wuhan University of Science and Technology, Wuhan, 430081, China

^cSchool of Electronic Information, Wuhan University of Science and Technology, Wuhan, 430081, China

^dHelmholtz-Zentrum Dresden-Rossendorf, Freiberg, 09599, Germany

^eSchool of Computer Science, Wuhan University, Wuhan, 430072, China

ARTICLE INFO

Keywords:

Multispectral images

Pretraining

Foundation model

Remote sensing

ABSTRACT

Pretraining and fine-tuning have emerged as a new paradigm in remote sensing image interpretation. Among them, Masked Autoencoder (MAE)-based pretraining stands out for its strong capability to learn general feature representations via reconstructing masked image regions. However, applying MAE to multispectral remote sensing images remains challenging due to complex backgrounds, indistinct targets, and the lack of semantic guidance during masking, which hinders the learning of underlying structures and meaningful spatial-spectral features. To address this, we propose a simple yet effective approach, Spectral Index-Guided MAE (SIGMAE), for multispectral image pretraining. The core idea is to incorporate domain-specific spectral indices as prior knowledge to guide dynamic token masking toward informative regions. SIGMAE introduces Semantic Saliency-Guided Dynamic Token Masking (SSDTM), a curriculum-style strategy that quantifies each patch's semantic richness and internal heterogeneity to adaptively select the most informative tokens during training. By prioritizing semantically salient regions and progressively increasing sample difficulty, SSDTM enhances spectrally rich and structurally aware representation learning, mitigates overfitting, and reduces redundant computation compared with random masking. Extensive experiments on five widely used datasets covering various downstream tasks, including scene classification, semantic segmentation, object extraction and change detection, demonstrate that SIGMAE outperforms other pretrained geospatial foundation models. Moreover, it exhibits strong spatial-spectral reconstruction capability, even with a 90% mask ratio, and improves complex target recognition under limited labeled data. The source codes and model weights will be released at <https://github.com/zxk688/SIGMAE>.

1. Introduction

Multispectral satellite images have been widely used for large-scale and continuous Earth observation applications like land use/cover mapping, natural resource management, environmental monitoring, and disaster assessment (Benhammou et al., 2022; Wang et al., 2023; Sun et al., 2024; Ghorbanzadeh et al., 2022; Zhang et al., 2023). A fundamental requirement for these applications is to efficiently and accurately capture desired information through image recognition and interpretation techniques. With the rise of deep learning, numerous models based on convolutional neural networks (CNNs) and Transformers have been proposed to learn discriminative feature representations (Zhang et al., 2016; Wu et al., 2021). Despite these efforts, these approaches still rely on large amounts of labeled data, and fully exploiting the rich spectral and spatial information in multispectral imagery remains a critical challenge (Tong et al., 2020; Zhang and Zhang, 2022).

The rapid advancement of self-supervised learning has driven the emergence of foundation models, establishing a new paradigm for geospatial applications (Xiao et al., 2025; Lu et al., 2025). By deriving supervisory signals directly from large-scale unlabeled data, pretraining strategies—such as contrastive learning (Li et al., 2022b; Guo et al., 2024) and masked image modeling (Jakubik et al., 2023; Mendieta et al., 2023; Noman et al., 2024)—alleviate the need for extensive human annotations. The pretrained models can subsequently be fine-tuned with only a limited number of labeled samples, significantly enhancing efficiency and adaptability in downstream Earth observation tasks (Ghamisi et al., 2025; Zhang et al., 2025).

✉ zhangxiaokang@whu.edu.cn (X. Zhang)
ORCID(s): 0000-0002-6127-4801 (X. Zhang)

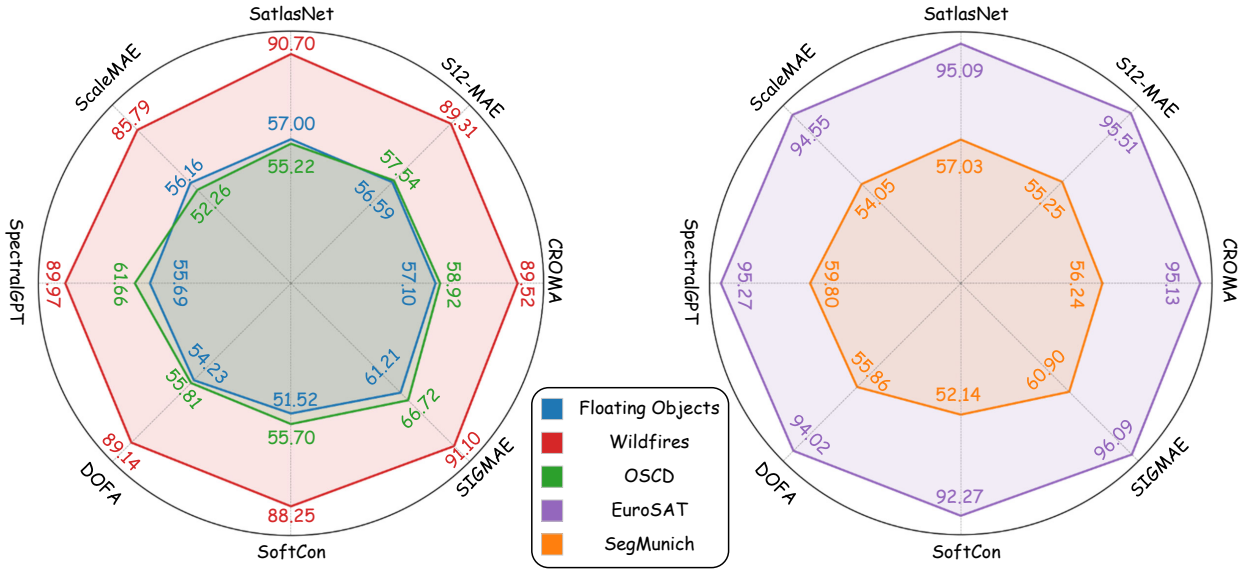


Figure 1: Performance comparison of remote sensing foundation models across five diverse datasets, where our SIGMAE achieved superior generalization capability.

Recent studies have demonstrated that masked image modeling (MIM) pretraining using *Masked Autoencoders* (MAE) models (He et al., 2022) is highly effective for enhancing image representation learning. The primary principle is to reconstruct the missing regions of an input image by utilizing compressed representations learned from visible patches through an encoder–decoder framework. Such a mechanism enables the model to capture contextual dependencies across image patches, which are crucial for various vision tasks. In the remote sensing domain, recent efforts have further extended MAE by introducing spectral-aware 3D Transformers (Hong et al., 2024), multi-scale modeling strategies (Noman et al., 2024), and spatial–temporal embeddings (Li et al., 2024; Cong et al., 2022), in order to more effectively capture the spatial and spectral properties of multispectral imagery. Despite its effectiveness in mining patterns from unlabeled data, MAE-based remote sensing image pretraining still faces several challenges that differ markedly from those in natural images.

1. Natural images used for MAE pretraining generally have clearer object boundaries and simpler backgrounds, which facilitate the learning process. In contrast, the targets in remote sensing images often exhibit semantic dispersion due to vague contours with complex and heterogeneous backgrounds.
2. The image reconstruction performance of MAE is highly related to the semantic components within the image (Li et al., 2022a; Chen et al., 2023). Since the entire training process lacks semantic knowledge and is inherently uncontrollable, MAE tends to learn general representations, and it is difficult to explicitly construct meaningful and semantic hints for masked modeling.
3. Vision Transformer-based segmentation models struggle to learn discriminative representations with limited labeled multispectral data due to their high parameter and token counts and computational demands (Hong et al., 2024). Moreover, most downstream tasks focus on common categories such as buildings, vegetation, and water, while complex targets with weak and diverse spectral signatures in moderate-resolution images remain underexplored.

To remedy these issues, we propose a novel spectral index-guided masked autoencoder (SIGMAE) for multispectral remote sensing image pretraining. Instead of the widely used random sampling strategy for patch masking, a dynamic masking method is proposed by leveraging remote sensing spectral indices as domain knowledge to guide the training process and enhance the model’s ability to capture informative spatial-spectral properties. The incorporation of domain knowledge into the pretrained model enhances its feature discriminative capability and facilitates its adaptation to a wide range of image interpretation downstream tasks. The main contributions of this work are as follows:

- A dynamic masking strategy that integrates remote sensing spectral indices as prior knowledge is developed to guide the masking process to focus on regions with rich spatial-spectral information, while facilitating discriminative representation learning.
- By adopting a curriculum learning manner and dynamically balancing the impacts of informative and less-informative patches in the masking process, SIGMAE enhances the model's ability to reason about semantic and global structural relationships during reconstruction while preserving variability to mitigate overfitting.
- The proposed approach achieved remarkable performance on various downstream tasks while requiring relatively few parameters and limited pretraining data.

2. Related Works

2.1. Remote Sensing Image Representation Learning

In remote sensing semantic segmentation tasks, Vision Transformer (ViT) and Swin Transformer (SwinT) have dominated due to their long-range context modeling capability by leveraging self-attention mechanisms, which allow them to focus on relevant areas of an image irrespective of their spatial distance (Hong et al., 2024; Ma et al., 2024). The ability of Transformers to effectively handle global contexts and maintain spatial relationships has been explored to capture multi-dimensional dependencies across spectral, spatial, and temporal dimensions for object extraction from multispectral images (Yuan et al., 2022; Schiller et al., 2024). To address the challenges of large-scale annotations for model training, the pretraining and fine-tuning paradigm has drawn sustained attention, with a large unlabeled set for self-supervised pretraining and then adapted to a specific task using a limited set of labeled data for fine-tuning (Tao et al., 2023; Mendieta et al., 2023; Bastani et al., 2023). Pretraining is typically conducted in a self-supervised learning manner, with methods such as contrastive learning (Diao et al., 2025; Guo et al., 2024; Xiong et al., 2024a; Wu et al., 2025) and masked image modeling (He et al., 2023). Self-supervised learning reduces dependence on labeled datasets by pretraining models on unlabeled data through intrinsic data patterns. It enables the model to learn robust representations, which can be fine-tuned with a few labeled samples to achieve strong performance on downstream tasks (Wang et al., 2022b; Xu et al., 2024).

2.2. MAE-based Pretraining

Recently, MAE has been investigated for self-supervised pretraining on large-scale, unlabeled remote sensing datasets. For high-resolution optical images, RVST (Wang et al., 2022a) applied MAE for pretraining large ViTs and introduced rotated, variable-size window attention to handle the large and arbitrarily oriented objects in remote sensing images. Moreover, RingMo (Sun et al., 2022) modified the MAE masking strategy by reversing some pixels in the masked patches to retain small objects. Furthermore, multi-scale pretraining has been developed considering the scale variation nature of remote sensing data by introducing cross-scale consistency constraints (Reed et al., 2023; Tang et al., 2024). For multispectral image modeling, SatMAE (Cong et al., 2022) focused on the spatial-temporal embedding of multitemporal and multispectral satellite images. For hyperspectral images, SpectralGPT (Hong et al., 2024) introduced a novel 3D generative transformer framework, while spatial-spectral properties have been explored in (Ibanez et al., 2022) and (Lin et al., 2023), respectively. SoftCon (Wang et al., 2024b) introduces a multi-label supervision framework with contrastive learning and a Siamese masking strategy to learn cross-scene soft similarities. More recently, multimodal and multitask pretraining of Vision Transformers have been investigated for remote sensing images (Fuller et al., 2024; Han et al., 2024; Wang et al., 2024a; Li et al., 2025). Our work differs from the aforementioned approaches by enhancing the masking strategy in MAE through the integration of remote sensing spectral indices, with a specific focus on complex target segmentation tasks.

2.3. Spectral Knowledge Guided Representation Learning

To integrate domain knowledge into semantic segmentation models, Li et al. (Li et al., 2022c) incorporated spectral indices such as NDBI, NDWI, and NDVI into the training process by introducing an additional decoder designed to reconstruct these indices and guide model learning. Alternatively, these indices can be treated as auxiliary input features and fused into multi-channel remote sensing composites (Tao et al., 2022; Audebert et al., 2018). In the context of pretraining, FG-MAE (Wang et al., 2025) employed multiple image features—such as edges, gradients, and normalized indices—as reconstruction targets, rather than the raw images. Nevertheless, explicitly reconstructing spectral indices or embedding them into the encoder during pretraining inevitably introduces substantial computational

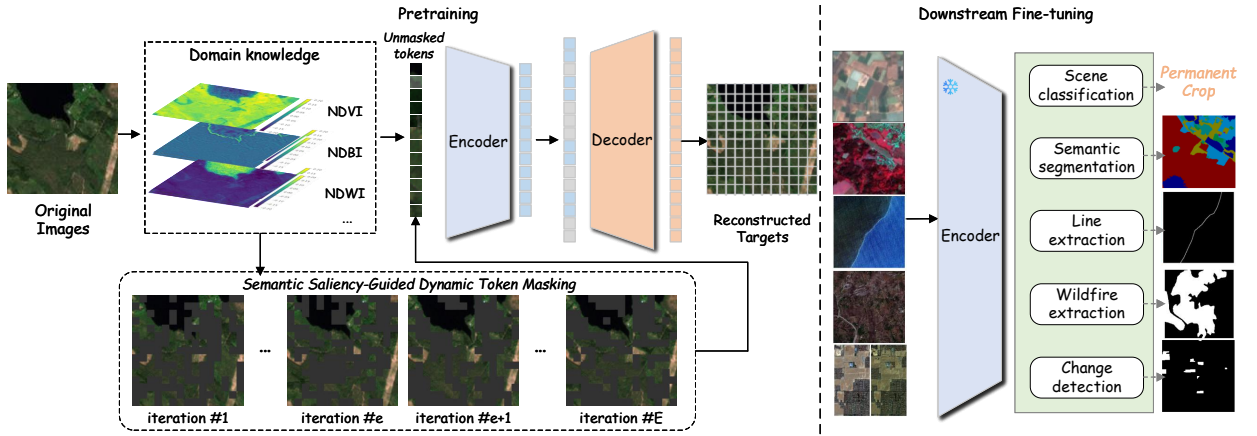


Figure 2: Overview of the proposed SIGMAE framework: an asymmetric encoder–decoder architecture equipped with Semantic Saliency-guided Dynamic Token Masking (SSDTM) that uses spectral-domain priors to adaptively select informative regions and enhance feature discriminability during reconstruction.

overhead and increases the complexity of training. In this article, we propose a more efficient way to incorporate the domain knowledge into the pretrained models.

3. Methods

3.1. SIGMAE Overview

SIGMAE adopts an asymmetric encoder-decoder structure grounded in Vision Transformers (ViT) (Dosovitskiy, 2020). In this framework, the encoder is designed to process only the visible subset of the input image and learn compact feature embeddings, while the decoder reconstructs the full image content by estimating the pixel values of the masked areas. In this study, we propose a dynamic semantic-guided masking strategy for selecting input tokens with spatially varied significance, as shown in Fig. 2.

3.1.1. Patchify

Let the input image be represented as $I \in \mathbb{R}^{C \times H \times W}$, where C denotes the number of channels, and H and W represent the spatial dimensions. The image is first partitioned into non-overlapping patches, resulting in a sequence $z \in \mathbb{R}^{L \times P^2 C}$, where each patch has size $P \times P$, and the number of patches is given by $L = \frac{H}{P} \cdot \frac{W}{P}$. These patches are embedded into a D -dimensional latent space through a linear projection $f_{proj} : \mathbb{R}^{P^2 C} \rightarrow \mathbb{R}^D$, producing patch tokens of the input image $\mathcal{Z} = \{z_1, z_2, \dots, z_L\}$.

3.1.2. Domain Knowledge Embeddings

Remote sensing spectral indices have been proven effective as prior domain knowledge to enhance the image representation capability (Li et al., 2022c; Wang et al., 2025). Typical spectral indices derived from remote sensing images are incorporated into the pretraining to exploit the distinctive properties of different spectral bands, providing valuable prior domain knowledge. Following previous works, the three most commonly used indices, NDVI, NDWI, and NDBI, are adopted in this study, which are highly responsive to vegetation, water bodies, and built-up areas, respectively.

To achieve domain knowledge embeddings, the spectral index values are first calculated from the input tensor using a patch-based approach. Let $\psi \in \mathbb{R}^{K \times H \times W}$ represent the concatenated spectral index tensor, where K is the number of indices. After that, we can compute the patch-level index with a patch size of $P \times P$, resulting in domain knowledge embeddings $\mathcal{A} \in \mathbb{R}^{K \times P^2 \times L}$.

3.1.3. Semantic Saliency-Guided Dynamic Token Masking (SSDTM)

Normally, for L tokens in \mathcal{Z} , a random masking strategy is applied such that a portion p_m of the tokens is concealed. The remaining $(1 - p_m)L$ visible tokens, enriched with positional encodings, are forwarded to the encoder to extract

meaningful representations. In comparison, SIGMAE adopts a dynamic token masking strategy through the dynamic adjustment of semantically rich patches and informative ones during the training process.

After that, we calculate the mean $\mu = \{\mu^k(\mathcal{A})\}_{k=1}^K$ and standard deviation $\sigma = \{\sigma^k(\mathcal{A})\}_{k=1}^K$ of knowledge embeddings within each patch. Specifically, the mean reflects both the dominant land cover and semantic certainty of a patch, where the sign determines the surface type while higher values imply richer semantic information, making the patch physically interpretable and showing stronger class discriminability. The standard deviation characterizes the heterogeneity within a patch, representing the reconstruction difficulty and measuring the degree of information dispersion within the patch. On this basis, considering the spectral polarity characteristic of remote sensing indices where both positive and negative values convey high semantic importance, we utilize a Semantic Saliency Measurement (SSM) to measure the semantic importance of each patch, which is defined as follows:

$$Q(\mathcal{A}_i) = \frac{1}{K} \sum_k \frac{\mu^k(|\mathcal{A}_i|)}{\sqrt{(\sigma^k(\mathcal{A}_i))^2 + \epsilon}}, \quad (1)$$

where ϵ is a small constant used to avoid division by zero. A higher SSM indicates that the patch contains richer and more discriminative semantic information with lower internal heterogeneity, thus being more suitable for reconstruction and model training. Conversely, a lower SSM implies sparse semantic information and high internal heterogeneity, resulting in greater reconstruction difficulty. Nevertheless, these patches contribute significantly to providing discriminative features for model training.

At each epoch, the dynamic masking score S for each token is computed by combining the SSM values and random noise, which can be expressed by:

$$S(\mathcal{A}_i, e) = \begin{cases} (1 - 2\gamma(e))Q(\mathcal{A}_i) + 2\gamma(e)v, & 0 < \gamma(e) \leq 0.5 \\ -\gamma(e)Q(\mathcal{A}_i) + (1 - \gamma(e))v, & 0.5 < \gamma(e) \leq 1 \end{cases} \quad (2)$$

where $\gamma(e) = e/E$ is a dynamic scaling factor that evolves over epochs indexed by e , where E is the total number of epochs and $v \sim \mathcal{U}(0, 1)$ represents the random noise, sampled uniformly from the range $[0, 1]$.

By adopting a curriculum learning paradigm, our method explicitly defines sample difficulty based on the mean and standard deviation of knowledge embeddings. By dynamically modulating the focus through $\gamma(e)$, this strategy establishes a distinct ‘Simple-to-Random-to-Hard’ progression: guiding the model from capturing dominant semantic features, through a stochastic transition, to focusing on subtle details. This content-aware schedule prevents early overfitting while ensuring later robustness, thereby demonstrating superior feature discriminability compared to static stochastic strategies.

To determine which tokens should be masked, we rank the tokens based on their dynamic scores, as follows:

$$\mathbf{T}^S = \left\{ i \mid i \in \text{top}_{\lfloor p_m \times L \rfloor} \left(\{S(\mathcal{A}_i)\}_{i=1}^L \right) \right\}, \quad (3)$$

where \mathbf{T}^S means the selected tokens to be masked and the binary mask can be obtained by:

$$\mathcal{M}_{\text{binary}} = \mathbb{1} \left\{ (h, w) \in \bigcup_{i \in \mathbf{T}^S} z_i \right\}, \quad (4)$$

where $\mathcal{M}_{\text{binary}}$ is a binary mask and $\mathbb{1}$ is an indicator function.

3.1.4. Pretraining

To recover the original image, the decoder takes all L token positions as input: the visible ones are inserted back into their original locations, while the masked positions are filled with a trainable mask token. Positional encodings are again incorporated to guide the reconstruction process. The decoder then produces the output $\hat{\mathcal{I}} \in \mathbb{R}^{C \times H \times W}$, aiming to reconstruct the original image as accurately as possible.

The model is trained by minimizing the reconstruction loss between the original image \mathcal{I} and the predicted reconstruction $\hat{\mathcal{I}}$, focusing only on the masked pixels. The reconstruction loss \mathcal{L}_{MAE} is typically computed using the mean squared error (MSE) between the original and reconstructed values at the masked positions:

$$\mathcal{L}_{\text{MAE}} = \frac{1}{|\mathcal{M}|} \sum_{h,w} \mathcal{M}_{h,w} \cdot (\mathcal{I}_{h,w} - \hat{\mathcal{I}}_{h,w})^2, \quad (5)$$

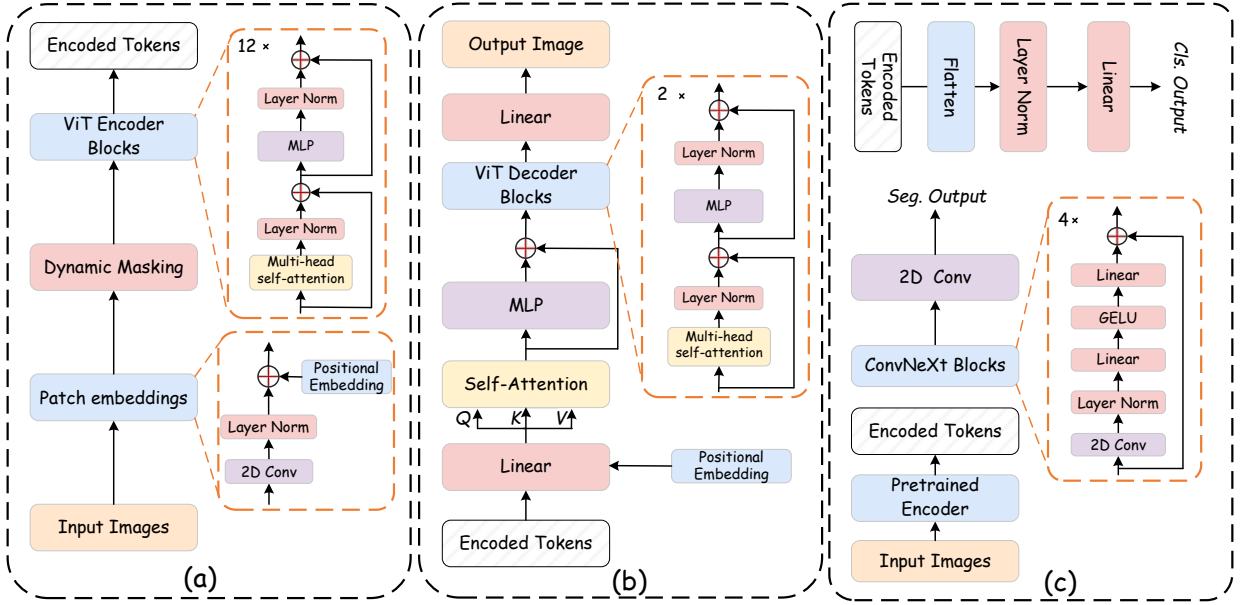


Figure 3: Details of network structures of the (a) encoder, (b) reconstruction decoder and (c) for downstream tasks.

where $\mathcal{M}_{h,w}$ is the mask value at position (h, w) , and $|\mathcal{M}|$ is the total number of masked pixels (i.e., where $\mathcal{M}_{h,w} = 1$). This ensures that only the masked pixels contribute to the loss computation. The details of the pretraining process are illustrated in Algorithm 1.

Algorithm 1: SIGMAE Pretraining

Input: \mathcal{I} : input image; ψ : spectral index tensor; p_m : mask ratio; P : patch size; E : total number of epochs; η : learning rate; θ : network parameters

Output: Pretrained network parameters θ

- 1 **for** $e = 1, \dots, E$ **do**
 - 2 Split \mathcal{I} into non-overlapping patches: $\mathcal{Z} \leftarrow \text{Patchify}(\mathcal{I}, P)$;
 - 3 Spectral knowledge embedding: $[\mu; \sigma] \leftarrow (\psi, P)$;
 - 4 Calculate masking score \mathcal{S} according to Eq. 2;
 - 5 Generate binary mask: $\mathbf{T}^S \leftarrow \left\{ \mathcal{A}_i \mid i \in \text{top}_{\lfloor p_m \times L \rfloor} \left(\left\{ \mathcal{S}(\mathcal{A}_i) \right\}_{i=1}^L \right) \right\}$;
 - 6 Obtain visible tokens: $\mathcal{Z}_v \leftarrow \mathcal{Z} \setminus \mathbf{T}^S$;
 - 7 Encode visible tokens: $\mathbf{h}_e \leftarrow \text{Encoder}(\mathcal{Z}_v)$;
 - 8 Decode full sequence: $\mathbf{h}_d \leftarrow \text{Decoder}(\mathbf{h}_e, \mathcal{M}_{\text{binary}})$;
 - 9 Predict original patches: $\hat{\mathcal{Z}} \leftarrow \text{ProjectionHead}(\mathbf{h}_d)$;
 - 10 Update parameters: $\theta \leftarrow \theta - \eta \cdot \nabla_{\theta} \mathcal{L}_{\text{MAE}}$;
-

3.2. Network Structures

The details of network structures in SIGMAE are illustrated in Fig. 3. A ViT-based autoencoder is adopted with an encoder and a reconstruction decoder.

First, 16×16 image patches are projected into tokens with the appropriate Transformer dimension. These projected patches are then concatenated into a token sequence. Pretrained weights can be directly loaded into a standard ViT by adjusting the input projection accordingly. After the linear projection, 2D sine–cosine positional embeddings are added before dynamic masking.

Table 1

Summary of datasets used in the downstream tasks

Dataset	Task	Image Size	Fine-tuning	Testing
FOD	Seg.	224 × 224	6,087	3,704
Wildfire Detection	Seg.	224 × 224	2,263	4,053
EuroSAT	Cls.	64 × 64	21,600	5,400
SegMunich	Seg.	128 × 128	39,402	9,846
OSCD	CD	224 × 224	7,160	3600

The decoder receives the full set of visible tokens as input. These visible tokens are jointly decoded along with a set of mask tokens, which act as placeholders allowing the decoder to reconstruct the masked patches from the visible ones. As illustrated in Fig. 3, the decoding process begins with a linear projection layer that aligns the dimensionality of the encoder output tokens with that of the decoder. Sine—cosine positional embeddings are then added to preserve spatial structure. The enriched tokens are subsequently fed into a stack of self-attention and MLP layers, followed by multiple Transformer blocks, which progressively refine the feature representations.

3.3. Dataset for Pretraining

The BigEarthNet-S2 (Sumbul et al., 2019) dataset serves as a large-scale benchmark for foundation model pretraining. It contains 590,326 image patches of size 120 × 120 extracted from Sentinel-2 satellite imagery collected during summer over Austria, Belgium, Finland, Ireland, Lithuania, Serbia, and Switzerland. Each patch is annotated with multiple land-cover labels derived from the CORINE Land Cover Map. For pretraining, ten Sentinel-2 bands were employed, excluding the two 60 m resolution bands that are primarily intended for atmospheric correction, cirrus detection, and cloud screening. The remaining 20 m resolution bands were upsampled to 10 m using nearest-neighbor interpolation to ensure spatial consistency across all bands.

3.4. Fine-Tuning

To support multiple downstream tasks, the unified token representation is routed to task-specific heads. For image-level classification, the token sequence is flattened and normalized before being mapped to category logits through a linear classifier, enabling efficient global prediction. To fine-tune the pretrained encoder for the image segmentation task, ConvNeXt (Liu et al., 2022), constructed from a pure convolutional net, is adopted as the segmentation head, as shown in Fig. 3. Leveraging patch-wise stems, inverted bottlenecks, and large kernels, ConvNeXts achieves competitive accuracy and scalability compared to transformers. More specifically, the output tokens are first passed through a linear projection to increase their dimensionality. After processing through ConvNeXt blocks, the feature map is upsampled back to the original image resolution using bilinear interpolation. For change detection, the two input images are fed through the same pretrained encoder, and their multi-level features are extracted and fused. Specifically, the corresponding intermediate representations from the four encoder stages are concatenated and subsequently provided to the decoder as its input.

4. Experiments

4.1. Benchmark Datasets

To assess the effectiveness of the pretrained foundation models, we conduct experiments on five datasets covering four downstream remote sensing tasks: scene classification, object extraction, semantic segmentation, and change detection. Beyond commonly used datasets, we also consider more challenging targets, such as floating objects and wildfire-affected areas, which are difficult to detect due to their weak and diverse spectral signatures in moderate-resolution imagery. The detailed settings of datasets in the downstream tasks are listed in Table 1.

4.1.1. Floating Objects Detection (FOD) Dataset

This dataset is designed for detecting floating objects on the sea surface using globally available medium-resolution Sentinel-2 imagery (Mifdal et al., 2021). It includes six categories of floating objects: plastic, pumice, seafoam, seawater, seaweed, and timber. This large-scale global data has a high diversity of floating objects, containing a dataset covering several coastal regions, such as Panama, Lagos, and Shengsi. In the experiments, all images were clipped into

Table 2

Foundation models used in benchmarking, with architecture, pretraining data, strategy, size, patch volume, and release year.

Model	Arch.	Pretrained EO Data	Learning Strategy	Params (M)	Patch Volume
CROMA (NIPS'24)	ViT	SSL4EO-S12 (Wang et al., 2023)	Contrastive	396.13	3M
SatlasNet (ICCV'23)	Swin-T	SatlasPretrain (Bastani et al., 2023)	Supervised	128.57	856K
S12-MAE (GRSM'23)	ViT	SSL4EO-S12 (Wang et al., 2023)	MIM	61.99	3M
ScaleMAE (ICCV'23)	ViT	fMoW-RGB (Christie et al., 2018)	MIM	396.21	363.6K
SpectralGPT (TPAMI'24)	ViT	fMoW-S2, BigEarthNet (Sumbul et al., 2019)	MIM	614.75	1.47M
SoftCon (TGRS'24)	ViT	SSL4EO-S12 (Wang et al., 2023)	Contrastive	242.19	3M
DOFA (arXiv'24)	ViT	DOFA (Xiong et al., 2024b)	MIM	178.20	8.08M
SIGMAE (Ours)	ViT	BigEarthNet (Sumbul et al., 2019)	MIM	118.90	54.9K

patches with a size of 224×224 pixels with a 64-pixel overlap. The training and test sets were split according to the coastal regions with a ratio of 2:1.

4.1.2. Wildfire Detection Dataset

The wildfire detection dataset (Arnaudo et al., 2023) includes Sentinel-2 imagery associated with wildfires, along with delineation masks, covering June 2017 to April 2023. The dataset includes 73 forest wildfires recorded between 2017 and 2019 across different regions in Europe. It covers a total area of approximately 19,000 km², featuring diverse terrain and morphological characteristics. Therefore, this dataset provides a robust benchmark for wildfire-related segmentation tasks. In the experiments, all images were clipped into patches of size 224×224 without overlaps. In the experiments, a limited number of samples are employed for fine-tuning, whereas a larger set is reserved for testing.

4.1.3. EuroSAT (Helber et al., 2019)

The EuroSAT dataset contains 27,000 Sentinel-2 satellite images collected from 34 European countries, each spanning 64×64 pixels with 13 spectral bands. The images are labeled into 10 land use classes, including Industrial Buildings, Residential Buildings, Annual Crop, Permanent Crop, Sea & Lake, Herbaceous Vegetation, Highway, Pasture and Forest, with each class comprising between 2,000 and 3,000 samples. The dataset is partitioned into training and test subsets using an 8/2 split.

4.1.4. SegMunich (Hong et al., 2024)

The dataset is constructed as a 10-band best-pixel composite with a spatial resolution of 10 m, covering an area of $3,847 \times 2,958$ pixels over a three-year period up to April 2020. It provides a segmentation mask that delineates 13 land-cover classes within the Munich metropolitan region, including categories such as arable land, pastures, forests, surface water, shrubland, and wetlands. The imagery is partitioned into patches of 128×128 pixels with 50% overlap, and subsequently divided into training and validation sets in an 8:2 ratio.

4.1.5. OSCD (Daudt et al., 2018)

The Onera Satellite Change Detection (OSCD) dataset is a benchmark designed for evaluating urban change detection methods using multispectral satellite imagery. It contains 24 pairs of co-registered Sentinel-2 images, each spanning 13 spectral bands, acquired between 2015 and 2018 from diverse regions worldwide, including Europe, the Middle East, Asia, the USA, and Brazil. Each image pair has a spatial size of 600×600 pixels, with resolution varying from 10 m to 60 m depending on the spectral band. Pixel-level change annotations are provided for 14 training pairs and 10 test pairs, highlighting urban transformations such as the development of new buildings or roads. All images were clipped into patches of size 224×224 with 40% overlaps.

4.2. Experimental Setup

The proposed approach was compared with several state-of-the-art foundation models, including SatlasNet (Bastani et al., 2023), S12-MAE from SSL4EO-S12 (Wang et al., 2023), CROMA (Fuller et al., 2024), SpectralGPT (Hong et al., 2024), DOFA (Xiong et al., 2024b) and ScaleMAE (Reed et al., 2023) to evaluate its performance. The architecture, pretraining data, strategy, model size, and patch volume of the compared foundation models are summarized in Table 2.

Table 3
Parameter Settings in the Pretraining and Fine-tuning.

Hyperparameters	Pretraining	Fine-tuning
Optimizer	AdamW	AdamW
Base learning rate	1e-4	1e-4
Weight decay	0.05	0.001
Adam β	(0.9, 0.95)	(0.9, 0.999)
Layer-wise lr decay	–	0.75
Batch size	900	20
Learning rate sched.	Cosine decay	Cosine decay
Training epochs	1000	50
Warmup learning rate	1e-6	1e-6
Warmup epochs	20	1
Non-masked tokens	112	–
Input resolution	120 × 120	e.g., 224 × 224

Table 4
Quantitative Results on FOD, Wildfires, OSCD, and EuroSAT Datasets for Segmentation, Change Detection, and Classification Tasks (%)

Model	FOD				Wildfires Detection				OSCD				EuroSAT		
	mIoU	F1	Recall	Precision	mIoU	F1	Recall	Precision	mIoU	F1	Recall	Precision	mIoU	OA	mF1
CROMA	57.10	62.87	72.68	59.05	89.52	89.52	95.59	84.18	58.92	66.98	76.53	62.80	95.13	97.61	97.49
S12-MAE	56.59	62.09	60.58	64.15	89.31	89.28	84.59	94.53	57.54	65.09	76.72	60.90	95.51	97.85	97.73
SatlasNet	57.00	62.79	62.62	62.98	90.70	90.78	94.96	86.96	55.22	61.58	87.67	57.39	95.09	97.59	97.44
ScaleMAE	56.16	61.49	67.24	58.66	85.79	85.25	82.15	88.60	52.26	57.09	72.60	54.70	94.55	97.25	97.14
SpectralGPT	55.69	60.68	74.28	56.93	89.97	90.00	85.44	95.07	61.66	70.50	79.49	63.30	95.27	97.94	97.72
DOFA	54.23	58.35	66.76	55.63	89.14	89.09	84.44	94.29	55.81	63.00	67.40	60.56	94.02	96.98	96.86
SoftCon	51.52	53.56	64.61	52.12	88.25	88.07	85.12	91.22	55.70	62.40	78.96	58.36	92.27	96.09	95.93
SIGMAE	61.21	68.87	76.54	64.72	91.10	91.02	92.92	90.21	66.72	76.33	78.29	74.65	96.09	98.09	97.99

Most of these models adopt transformer-based architectures, with ViT (Dosovitskiy, 2020) being a representative choice. Their sizes range from 61.99M to 614.75M parameters, and the patch volumes vary from 54.9K to 8.08M, reflecting different levels of spatial granularity considered during pretraining. Specifically, S12-MAE and CROMA are pretrained on 3 million samples from Sentinel-2 and Sentinel-1 imagery, while SatlasNet is trained in a fully supervised manner with 856K samples. SpectralGPT, on the other hand, leverages fMoW-S2 (Christie et al., 2018) and BigEarthNet (Sumbul et al., 2019) with the largest model size among them. In contrast, SIGMAE is characterized by a comparatively compact model size and the minimal patch volume, underscoring its efficiency in representation learning. For all baseline methods, we employ the publicly released weights before fine-tuning on the labeled datasets.

For quantitative evaluation, five commonly used metrics were employed: overall accuracy (OA), precision, recall, F1-score, and mean intersection over union (mIoU). The parameter settings of the SIGMAE pretraining and fine-tuning are displayed in Table 3, respectively. All models were implemented using the PyTorch framework. The experiments were conducted on an Ubuntu operating system equipped with four NVIDIA A100 Tensor Core GPUs.

4.3. Quantitative Analysis

The quantitative results presented in Tables 4 and 5 highlight the superior performance of the proposed SIGMAE among existing models.

Table 4 reports the quantitative results on the Floating Objects detection, Wildfire detection, OSCD and EuroSAT datasets. The results indicate that the competing methods achieve leading scores only on a few isolated metrics or datasets. For example, CROMA attains the highest Recall on Wildfires, SatlasNet achieves the best Recall on OSCD, and SpectralGPT provides the highest Precision on Wildfires. In contrast, the proposed SIGMAE consistently

Table 5
Quantitative Results on SegMunich Dataset (%)

Method	Background	Arable land	Perm. Crops	Pastures	Forests	Surface water	Shrub	Open spaces	Wetlands	Mine, dump	Artificial veg.	Urban fabric	Buildings	mF1
CROMA	90.64	82.77	21.42	64.07	89.12	70.51	20.62	33.32	44.72	40.57	27.79	78.33	67.25	56.24
S12-MAE	89.48	81.89	22.25	62.24	88.51	71.25	16.73	34.80	44.08	40.94	25.51	76.32	64.25	55.25
SatlasNet	90.81	81.69	17.98	61.32	88.43	81.30	16.45	43.81	50.44	47.08	22.44	75.93	63.69	57.03
ScaleMAE	85.12	81.14	20.04	60.82	87.62	70.49	15.77	29.45	44.29	39.47	25.52	77.32	65.57	54.05
SpectralGPT	87.80	83.34	31.24	65.53	89.11	85.84	21.31	46.05	46.41	52.59	23.98	78.97	65.18	59.80
DOFA	89.91	81.97	21.51	62.41	88.65	71.09	18.71	33.04	43.11	39.78	27.99	77.57	66.21	55.86
SoftCon	89.77	88.51	11.21	64.58	88.89	62.52	11.76	24.11	34.70	30.55	20.12	82.11	68.93	52.14
SIGMAE	90.14	81.09	32.71	63.65	89.37	85.09	22.26	48.88	55.15	50.51	31.31	77.05	64.47	60.90

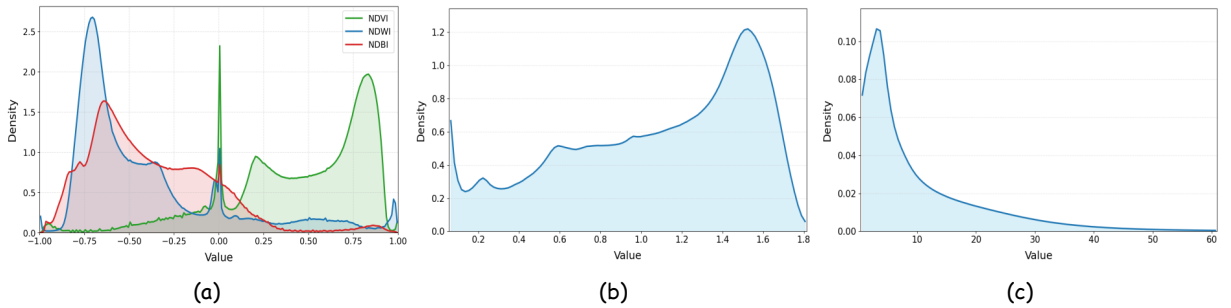


Figure 4: Statistical characterization of spectral attributes and patch-level saliency indicators in BigEarthNet-S2 dataset. (a) Probability density functions of raw spectral indices (NDVI, NDWI, and NDBI) within the BigEarthNet-S2 dataset. (b) Distribution of the sum of absolute values derived from the indices, representing semantic richness. (c) Probability density of the resulting SSM.

delivers superior performance across most metrics, achieving the highest mIoU, F1, and Precision on Floating Objects, the highest mIoU and F1 on Wildfires, and the best overall results on OSCD. These results demonstrate the generalization ability of SIGMAE across different remote sensing tasks. For the image classification task on the EuroSAT dataset, SIGMAE obtains the best mIoU with comparable performance on the metrics, demonstrating its overall competitiveness.

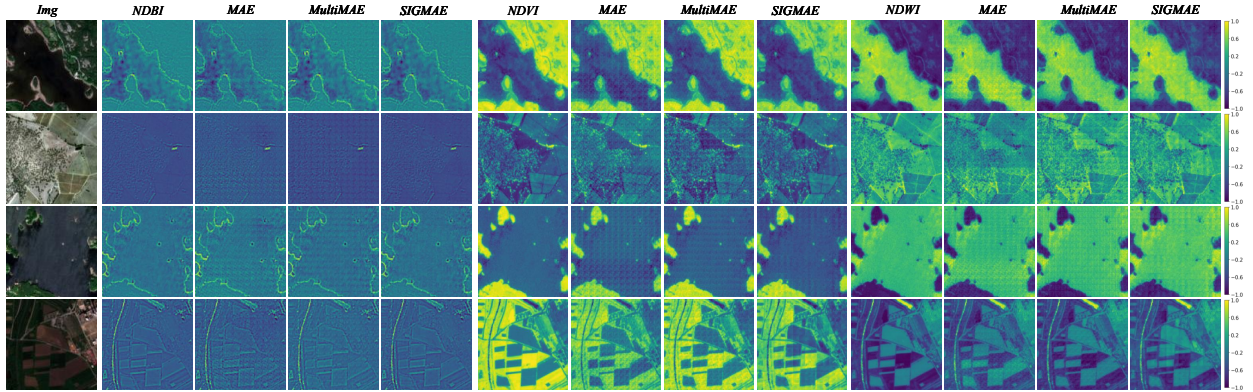
Table 5 presents the quantitative performance of different methods on the SegMunich dataset across 13 land-cover categories, reported in terms of F1-scores. As observed, the results show that existing approaches achieve the best performance only in a few individual categories, but fail to deliver competitive results across all classes. For example, SatlasNet achieves the highest performance in Background and Surface water, while SpectralGPT leads in Pastures, Surface water, and Mine, dump. In contrast, the proposed SIGMAE consistently attains strong performance in multiple categories, including Permanent crops, Forests, Shrub, Open spaces, Wetlands, Artificial vegetation, and achieves the highest mean F1-score, demonstrating its superior overall effectiveness and robustness.

4.4. Interpretability analysis

This comprehensive statistical characterization, as visualized in Fig. 4, forms the foundation of our masking strategy. Specifically, Fig. 4 (a) illustrates the distribution of raw remote sensing indices and their coupling relationships across diverse environments. To quantify the information density, the semantic richness of the knowledge embeddings is explicitly derived by summing the absolute values of these remote sensing indices as presented in Fig. 4 (b). By calculating the ratio of this semantic richness to the standard deviation, we derive the SSM for each patch. As illustrated in Fig. 4 (c), compared to the distribution of remote sensing indices in Fig. 4 (a) and the semantic richness in Fig. 4 (b),

Table 6
Ablation Studies (%)

Model Variants	FOD		Wildfire		EuroSAT		SegMunich		OSCD	
	mIoU	F1	mIoU	F1	mIoU	mF1	mIoU	mF1	mIoU	F1
SIGMAE w/o SSDTM	59.19	65.96	89.92	89.96	94.54	97.15	46.16	59.98	65.04	74.51
MAE w/ Index Fusion	59.70	67.03	89.06	89.04	95.16	97.50	46.31	59.96	64.96	74.44
SIGMAE w/o $\gamma(e)$	61.23	68.78	90.67	90.73	94.58	97.18	46.44	60.16	66.07	75.70
SIGMAE (Full)	61.21	68.87	91.12	91.20	95.53	97.70	47.45	60.90	65.45	75.03

**Figure 5:** Spectral reconstruction performance comparison.

the SSM exhibits a distinct and typical long-tail distribution. Only a tiny fraction of patches possess extremely high SSM values; while scarce in number, these patches are semantically “pure”, allowing the model to anchor fundamental spatial-spectral mapping relationships by prioritizing the reconstruction of these “elite” few.

4.5. Ablation Studies

To verify the effectiveness of the proposed dynamic masking and knowledge injection strategies, we conduct ablation studies on SIGMAE by comparing it with the original MAE (He et al., 2022), fusion-based MAE that incorporates spectral indices as an additional modality (Bachmann et al., 2022), and a SIGMAE variant without random noise. Compared with MAE and fusion-based MAE, both variants of SIGMAE achieve consistent improvements across all datasets, as shown in Table 6. Specifically, the introduction of the dynamic masking strategy $\gamma(e)$ leads to noticeable gains in mIoU and F1, indicating enhanced representation learning through adaptive feature reconstruction. The full version of SIGMAE, which integrates both dynamic masking and knowledge injection, achieves the highest performance in all metrics, demonstrating the effectiveness of the proposed strategies in improving model generalization and robustness across diverse remote sensing applications.

4.6. Reconstruction Performance

We have undertaken extensive investigations into the reconstruction performance of different models to validate the spectral modeling capability in the pretraining. From visual comparison of the reconstruction performance of different models, as shown in Fig. 5, SIGMAE exhibits superior reconstruction fidelity compared to MAE and MultiMAE. The evident visual discrepancies observed in the reconstruction are primarily attributed to spectral degradation caused by the relatively limited reconstruction and inference capacities of the MAE model. The reconstructions of SIGMAE retain sharper details and exhibit fewer distortions, particularly in regions characterized by complex textures and transitions.

4.7. Masking Ratio Analysis

We further provide visual comparisons across varying masking ratios (50%, 75%, and 90%) to assess the spectral reconstruction performance of SIGMAE. The capacity of the pre-training strategy to learn rich, generalized representations is visually confirmed by the reconstruction performance shown in Fig. 6. As the masking ratio increases

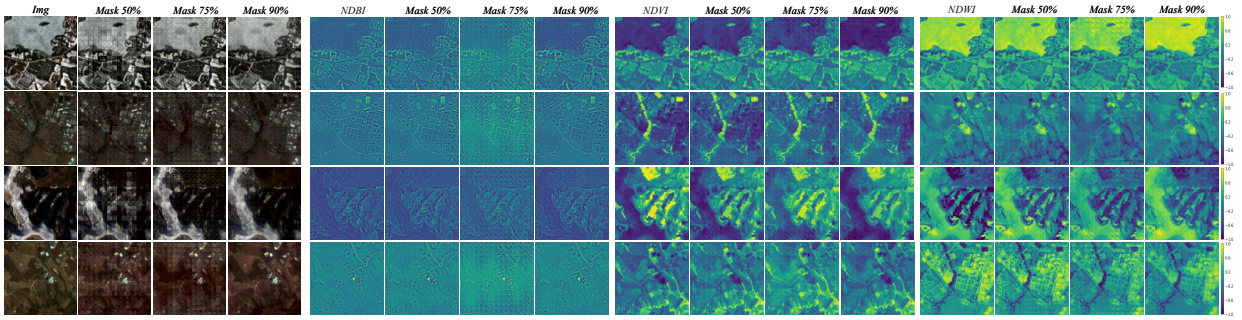


Figure 6: Image reconstruction performance comparison with varied masking ratios of 50%, 75% and 90%, respectively.

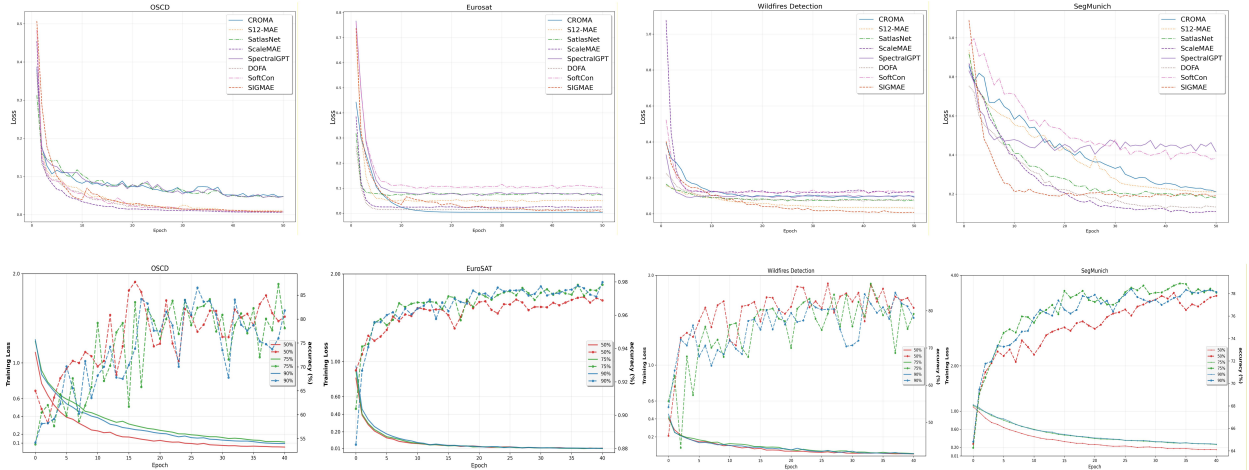


Figure 7: Convergence performance comparison with different models and different mask ratios.

from 50% to 90%, the reconstructed images maintain high fidelity, preserving structural continuity, fine-grained textures, and the characteristic intensity distribution of the indices. This robust reconstruction capability, particularly across multiple spectral indices, demonstrates that the model successfully learns the underlying spatial and spectral dependencies within the remote sensing data.

A 90% masking ratio leaves the model with very limited observable information, driving it to rely primarily on the global statistics or mean structure of the data. However, the model is still able to produce visually smooth and coherent reconstructions. However, the absence of sufficient contextual cues inevitably leads to the loss of fine-scale details. As a result, it converges more rapidly than models trained with lower masking ratios, as illustrated in Fig. 7. It shows that EuroSAT (classification) and SegMunich (large-area segmentation) gain from the high-ratio masking setting, whereas fine-grained datasets such as Wildfires and OSCD exhibit noticeably reduced performance.

4.8. Fine-Tuning Convergence

The fine-tuning loss curves across four datasets offer key insights into model stability and convergence. As shown in Fig. 7, the proposed SIGMAE achieves one of the fastest convergence rates, reducing loss rapidly within the first 10–15 epochs, especially on the EuroSAT and OSCD benchmarks. Moreover, SIGMAE maintains exceptional training stability, with smooth and consistent loss reduction and minimal oscillations, indicating robust optimization and effective regularization. In contrast, models such as SpectralGPT and SoftCon exhibit higher baseline losses and unstable convergence, with fluctuating or prematurely flattened loss curves (e.g., SoftCon on SegMunich). These results confirm that SIGMAE’s injection of prior knowledge supports stable, efficient learning and superior final optimization.

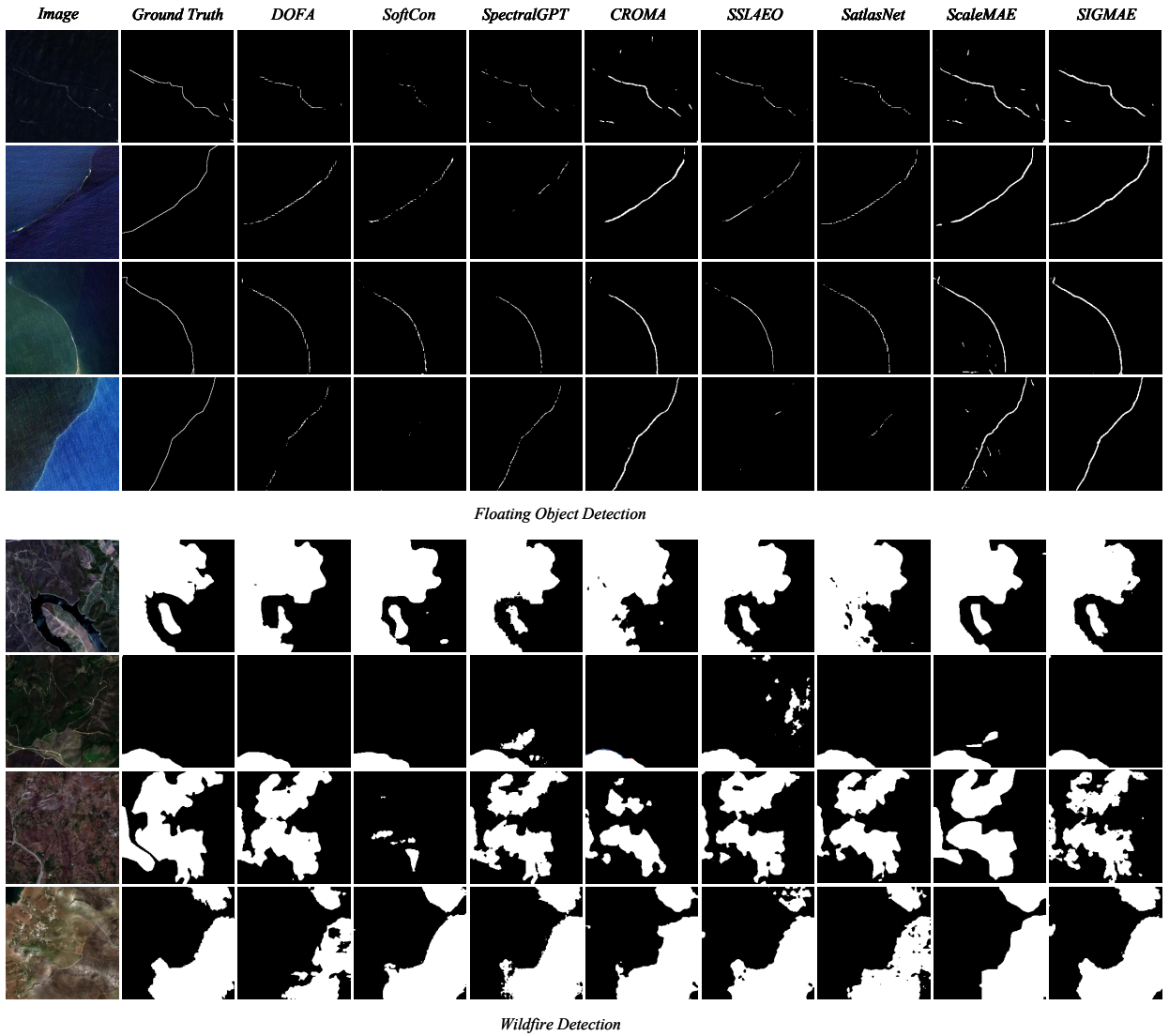


Figure 8: Segmentation performance on the Floating object detection and wildfire detection datasets.

4.9. Visual Comparison

The visual comparison of segmentation and classification results is displayed in Figs. 8, 9 and 10. In Floating Object Detection, where targets are primarily linear, competing methods such as SpectralGPT and SoftCon often produce fragmented masks, resulting in false negatives and compromised structure. SIGMAE, in contrast, generates continuous, high-precision boundaries closely matching the ground truth. For Wildfire Detection, involving complex, large-area wildfire areas, SIGMAE robustly delineates irregular boundaries with fewer internal voids or under-segmentation than DOFA and CROMA, highlighting its strong generalization and noise suppression capabilities.

In semantic segmentation on the SegMunich dataset, many methods struggle with fine-grained boundaries, resulting in jagged edges and misclassified small structures. SpectralGPT and AtlasNet produce blurred transitions and blocky artifacts between major classes such as “Forests” and “Arable land”. SIGMAE delivers precise, coherent masks while preserving small land cover patches like thin roads or fragmented “Permanent Crops”, leveraging both spectral and contextual information for accurate pixel-level classification.

For change detection on the OSCD dataset, which features small, isolated changes and spectral noise from atmospheric effects, DOFA, SoftCon, and ScaleMAE generate numerous false positives in background areas. SIGMAE

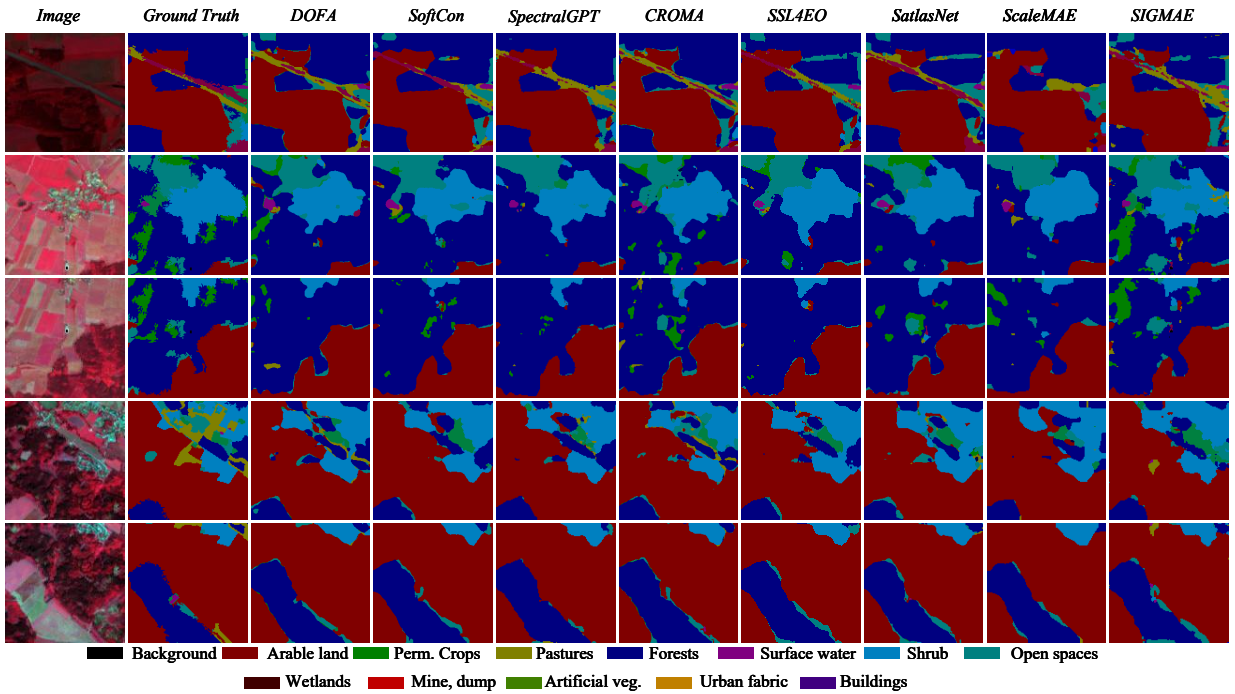


Figure 9: Semantic segmentation performance on the SegMunich dataset.

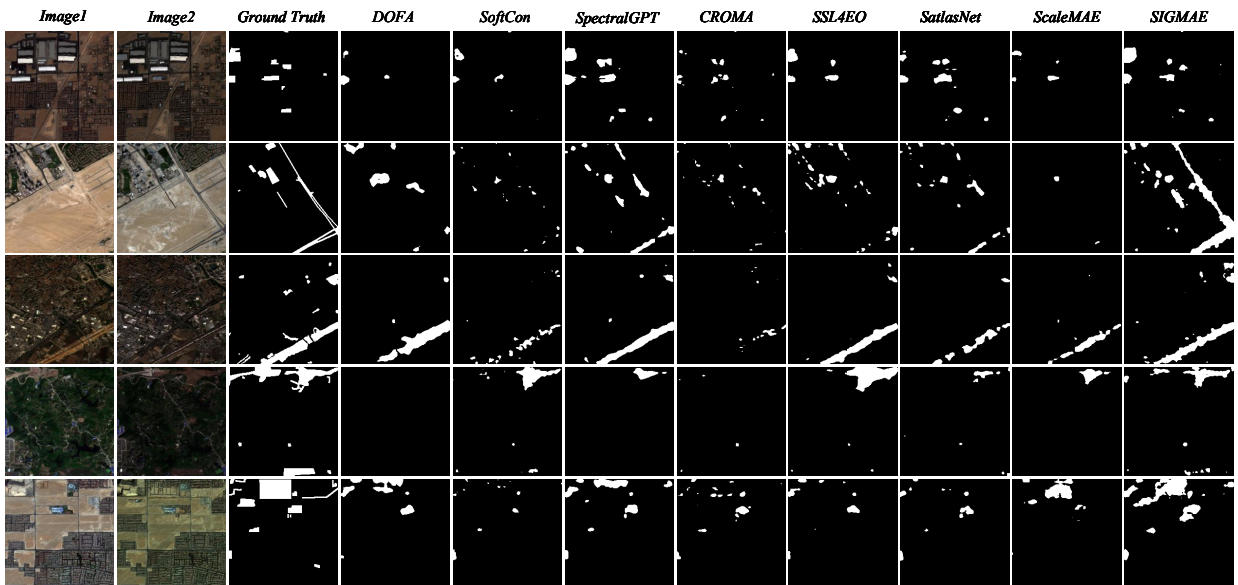


Figure 10: Change detection performance on the OSCD dataset.

mitigates this issue via its dynamic masking mechanism, producing clean change maps while maintaining sharp boundaries for small changes such as new buildings, achieving a superior balance between noise suppression and recall. Overall, SIGMAE consistently provides accurate and structurally coherent segmentation and detection across varied tasks and challenging conditions.

4.10. Scope and Limitations

The proposed SIGMAE focuses on pretraining of large-scale multispectral images by exploiting remote sensing index information to guide the masking process. Compared to the multimodal visual foundation (Guo et al., 2024), the limitation of SIGMAE lies in that it is specially designed for a single modality, i.e., multispectral images. Our goal is to explore an efficient pretraining and fine-tuning strategy on multispectral images. And the model performance inherently depends on the domain knowledge, namely, the spectral indices. For downstream tasks, we evaluate the performance of our method on several mainstream multispectral datasets. In future work, we plan to incorporate multimodal datasets for pre-training, which is expected to further enhance the robustness and generalization capability of SIGMAE across diverse Earth observation applications.

5. Conclusion

This paper proposed a novel spectral index-guided Masked Autoencoder (SIGMAE) to build a foundation model for multispectral remote sensing images. It deploys MAE-style self-supervised pretraining, followed by fine-tuning with a limited number of labeled samples. Meaningful spectral indices are incorporated as prior domain knowledge to enhance the feature representation of the target objects. Instead of directly reconstructing spectral indices or using them as additional model inputs, we propose a novel dynamic masking strategy that leverages spectral indices to replace the random sampling strategy used in the original MAE. By guiding the masking process towards informative regions during image reconstruction, this strategy improves the model's ability to capture essential object properties, ensuring that masked regions contribute to a more meaningful and informative learning process. Experiments on five large-scale datasets validate the effectiveness of the proposed approach. The results show that the proposed SIGMAE outperforms existing MAE-based methods in both spatial and spectral information reconstruction. More importantly, it learns more robust feature representations, leading to improved classification, segmentation and change detection performance. Future work will focus on extending the proposed dynamic masking strategy to multimodal remote sensing image pretraining, utilizing various domain-specific knowledge.

CRedit authorship contribution statement

Xiaokang Zhang: Conceptualization, Methodology, Writing - original draft, Funding acquisition. **Bo Li:** Data curation, Investigation, Software, Validation, Writing - review & editing. **Chufeng Zhou:** Data curation, Investigation, Software, Validation, Writing - review & editing. **Weikang Yu:** Data curation, Investigation, Software, Validation, Writing - review & editing. **Lefei Zhang:** Conceptualization, Methodology, Supervision, Writing - review & editing.

Declaration of competing interest

The authors declare that they have no known competing financial interests or personal relationships that could have appeared to influence the work reported in this paper.

Acknowledgments

This work was supported in part by the Open Research Fund from Guangdong Laboratory of Artificial Intelligence and Digital Economy (SZ) under Grant No. GML-KF-24-28, and in part by the National Natural Science Foundation of China under Grant No. 42371374.

References

- Arnaudo, E., Barco, L., Merlo, M., Rossi, C., 2023. Robust burned area delineation through multitask learning, in: Joint European Conference on Machine Learning and Knowledge Discovery in Databases, Springer. pp. 436–447.
- Audebert, N., Le Saux, B., Lefèvre, S., 2018. Beyond rgb: Very high resolution urban remote sensing with multimodal deep networks. *ISPRS journal of photogrammetry and remote sensing* 140, 20–32.
- Bachmann, R., Mizrahi, D., Atanov, A., Zamir, A., 2022. Multima: Multi-modal multi-task masked autoencoders, in: European Conference on Computer Vision, Springer. pp. 348–367.
- Bastani, F., Wolters, P., Gupta, R., Ferdinando, J., Kembhavi, A., 2023. Satlaspretrain: A large-scale dataset for remote sensing image understanding, in: Proceedings of the IEEE/CVF International Conference on Computer Vision, pp. 16772–16782.
- Benhammou, Y., Alcaraz-Segura, D., Guirado, E., Khaldi, R., Achchab, B., Herrera, F., Tabik, S., 2022. Sentinel2globalluc: A sentinel-2 rgb image tile dataset for global land use/cover mapping with deep learning. *Scientific Data* 9, 681.

- Chen, H., Zhang, W., Wang, Y., Yang, X., 2023. Improving masked autoencoders by learning where to mask, in: Chinese Conference on Pattern Recognition and Computer Vision (PRCV), Springer. pp. 377–390.
- Christie, G., Fendley, N., Wilson, J., Mukherjee, R., 2018. Functional map of the world, in: Proceedings of the IEEE Conference on Computer Vision and Pattern Recognition, pp. 6172–6180.
- Cong, Y., Khanna, S., Meng, C., Liu, P., Rozi, E., He, Y., Burke, M., Lobell, D., Ermon, S., 2022. Satmae: Pre-training transformers for temporal and multi-spectral satellite imagery. *Advances in Neural Information Processing Systems* 35, 197–211.
- Daudt, R.C., Le Saux, B., Boulch, A., Gousseau, Y., 2018. Urban change detection for multispectral earth observation using convolutional neural networks, in: IGARSS 2018-2018 IEEE International Geoscience and Remote Sensing Symposium, Ieee. pp. 2115–2118.
- Diao, W., Yu, H., Kang, K., Ling, T., Liu, D., Feng, Y., Bi, H., Ren, L., Li, X., Mao, Y., Sun, X., 2025. Ringmo-aerial: An aerial remote sensing foundation model with affine transformation contrastive learning. *IEEE Transactions on Pattern Analysis and Machine Intelligence* 47, 10900–10913. doi:10.1109/TPAMI.2025.3602237.
- Dosovitskiy, A., 2020. An image is worth 16x16 words: Transformers for image recognition at scale. arXiv preprint arXiv:2010.11929 .
- Fuller, A., Millard, K., Green, J., 2024. Croma: Remote sensing representations with contrastive radar-optical masked autoencoders. *Advances in Neural Information Processing Systems* 36.
- Ghamisi, P., Yu, W., Zhang, X., Rizaldy, A., Wang, J., Zhou, C., Gloaguen, R., Camps-Valls, G., 2025. Geospatial foundation models to enable progress on sustainable development goals. arXiv preprint arXiv:2505.24528 .
- Ghorbanzadeh, O., Xu, Y., Zhao, H., Wang, J., Zhong, Y., Zhao, D., Zang, Q., Wang, S., Zhang, F., Shi, Y., et al., 2022. The outcome of the 2022 landslide4sense competition: Advanced landslide detection from multisource satellite imagery. *IEEE Journal of Selected Topics in Applied Earth Observations and Remote Sensing* 15, 9927–9942.
- Guo, X., Lao, J., Dang, B., Zhang, Y., Yu, L., Ru, L., Zhong, L., Huang, Z., Wu, K., Hu, D., et al., 2024. Skysense: A multi-modal remote sensing foundation model towards universal interpretation for earth observation imagery, in: Proceedings of the IEEE/CVF Conference on Computer Vision and Pattern Recognition, pp. 27672–27683.
- Han, B., Zhang, S., Shi, X., Reichstein, M., 2024. Bridging remote sensors with multisensor geospatial foundation models, in: Proceedings of the IEEE/CVF Conference on Computer Vision and Pattern Recognition, pp. 27852–27862.
- He, K., Chen, X., Xie, S., Li, Y., Dollár, P., Girshick, R., 2022. Masked autoencoders are scalable vision learners, in: Proceedings of the IEEE/CVF conference on computer vision and pattern recognition, pp. 16000–16009.
- He, Q., Sun, X., Yan, Z., Wang, B., Zhu, Z., Diao, W., Yang, M.Y., 2023. Ast: Adaptive self-supervised transformer for optical remote sensing representation. *ISPRS Journal of Photogrammetry and Remote Sensing* 200, 41–54.
- Helber, P., Bischke, B., Dengel, A., Borth, D., 2019. Eurosat: A novel dataset and deep learning benchmark for land use and land cover classification. *IEEE Journal of Selected Topics in Applied Earth Observations and Remote Sensing* 12, 2217–2226.
- Hong, D., Zhang, B., Li, X., Li, Y., Li, C., Yao, J., Yokoya, N., Li, H., Ghamisi, P., Jia, X., Plaza, A., Gamba, P., Benediktsson, J.A., Chanussot, J., 2024. Spectralgpt: Spectral remote sensing foundation model. *IEEE Transactions on Pattern Analysis and Machine Intelligence* 46, 5227–5244. doi:10.1109/TPAMI.2024.3362475.
- Ibanez, D., Fernandez-Beltran, R., Pla, F., Yokoya, N., 2022. Masked auto-encoding spectral-spatial transformer for hyperspectral image classification. *IEEE Transactions on Geoscience and Remote Sensing* 60, 1–14.
- Jakubik, J., Roy, S., Phillips, C., Fraccaro, P., Godwin, D., Zadrozny, B., Szwarcman, D., Gomes, C., Nyirjesy, G., Edwards, B., et al., 2023. Foundation models for generalist geospatial artificial intelligence. arXiv preprint arXiv:2310.18660 .
- Li, G., Zheng, H., Liu, D., Wang, C., Su, B., Zheng, C., 2022a. Semmae: Semantic-guided masking for learning masked autoencoders. *Advances in Neural Information Processing Systems* 35, 14290–14302.
- Li, H., Li, Y., Zhang, G., Liu, R., Huang, H., Zhu, Q., Tao, C., 2022b. Global and local contrastive self-supervised learning for semantic segmentation of hr remote sensing images. *IEEE Transactions on Geoscience and Remote Sensing* 60, 1–14.
- Li, X., Hong, D., Chanussot, J., 2024. S2mae: A spatial-spectral pretraining foundation model for spectral remote sensing data, in: Proceedings of the IEEE/CVF Conference on Computer Vision and Pattern Recognition, pp. 24088–24097.
- Li, X., Li, C., Ghamisi, P., Hong, D., 2025. Fleximo: A flexible remote sensing foundation model. arXiv preprint arXiv:2503.23844 .
- Li, Y., Zhou, Y., Zhang, Y., Zhong, L., Wang, J., Chen, J., 2022c. Dkdfn: Domain knowledge-guided deep collaborative fusion network for multimodal unitemporal remote sensing land cover classification. *ISPRS Journal of Photogrammetry and Remote Sensing* 186, 170–189.
- Lin, J., Gao, F., Shi, X., Dong, J., Du, Q., 2023. Ss-mae: Spatial-spectral masked autoencoder for multisource remote sensing image classification. *IEEE Transactions on Geoscience and Remote Sensing* 61, 1–14.
- Liu, Z., Mao, H., Wu, C.Y., Feichtenhofer, C., Darrell, T., Xie, S., 2022. A convnet for the 2020s, in: Proceedings of the IEEE/CVF conference on computer vision and pattern recognition, pp. 11976–11986.
- Lu, S., Guo, J., Zimmer-Dauphinee, J.R., Nieuwsma, J.M., Wang, X., Wernke, S.A., Huo, Y., et al., 2025. Vision foundation models in remote sensing: A survey. *IEEE Geoscience and Remote Sensing Magazine* .
- Ma, X., Zhang, X., Pun, M.O., Liu, M., 2024. A multilevel multimodal fusion transformer for remote sensing semantic segmentation. *IEEE Transactions on Geoscience and Remote Sensing* 62, 1–15. doi:10.1109/TGRS.2024.3373033.
- Mendieta, M., Han, B., Shi, X., Zhu, Y., Chen, C., 2023. Towards geospatial foundation models via continual pretraining, in: Proceedings of the IEEE/CVF International Conference on Computer Vision, pp. 16806–16816.
- Mifdal, J., Longépé, N., Rufwurm, M., 2021. Towards detecting floating objects on a global scale with learned spatial features using sentinel 2. *ISPRS Annals of the Photogrammetry, Remote Sensing and Spatial Information Sciences* 3, 285–293.
- Noman, M., Naseer, M., Cholakkal, H., Anwer, R.M., Khan, S., Khan, F.S., 2024. Rethinking transformers pre-training for multi-spectral satellite imagery, in: Proceedings of the IEEE/CVF Conference on Computer Vision and Pattern Recognition, pp. 27811–27819.
- Reed, C.J., Gupta, R., Li, S., Brockman, S., Funk, C., Clipp, B., Keutzer, K., Candido, S., Uyttendaele, M., Darrell, T., 2023. Scale-mae: A scale-aware masked autoencoder for multiscale geospatial representation learning, in: Proceedings of the IEEE/CVF International Conference on Computer Vision, pp. 4088–4099.

- Schiller, C., Költzow, J., Schwarz, S., Schiefer, F., Fassnacht, F.E., 2024. Forest disturbance detection in central Europe using transformers and sentinel-2 time series. *Remote Sensing of Environment* 315, 114475.
- Sumbul, G., Charfuelan, M., Demir, B., Markl, V., 2019. Bigearthnet: A large-scale benchmark archive for remote sensing image understanding, in: IGARSS 2019 - 2019 IEEE International Geoscience and Remote Sensing Symposium, pp. 5901–5904. doi:10.1109/IGARSS.2019.8900532.
- Sun, J., Yan, S., Yao, X., Gao, B., Yang, J., 2024. A segment anything model based weakly supervised learning method for crop mapping using sentinel-2 time series images. *International Journal of Applied Earth Observation and Geoinformation* 133, 104085.
- Sun, X., Wang, P., Lu, W., Zhu, Z., Lu, X., He, Q., Li, J., Rong, X., Yang, Z., Chang, H., et al., 2022. Ringmo: A remote sensing foundation model with masked image modeling. *IEEE Transactions on Geoscience and Remote Sensing* 61, 1–22.
- Tang, M., Cozma, A., Georgiou, K., Qi, H., 2024. Cross-scale mae: A tale of multiscale exploitation in remote sensing. *Advances in Neural Information Processing Systems* 36.
- Tao, C., Meng, Y., Li, J., Yang, B., Hu, F., Li, Y., Cui, C., Zhang, W., 2022. Msnet: Multispectral semantic segmentation network for remote sensing images. *GIScience & Remote Sensing* 59, 1177–1198.
- Tao, C., Qi, J., Guo, M., Zhu, Q., Li, H., 2023. Self-supervised remote sensing feature learning: Learning paradigms, challenges, and future works. *IEEE Transactions on Geoscience and Remote Sensing* 61, 1–26.
- Tong, X.Y., Xia, G.S., Lu, Q., Shen, H., Li, S., You, S., Zhang, L., 2020. Land-cover classification with high-resolution remote sensing images using transferable deep models. *Remote Sensing of Environment* 237, 111322.
- Wang, D., Zhang, J., Xu, M., Liu, L., Wang, D., Gao, E., Han, C., Guo, H., Du, B., Tao, D., Zhang, L., 2024a. Mtp: Advancing remote sensing foundation model via multitask pretraining. *IEEE Journal of Selected Topics in Applied Earth Observations and Remote Sensing* 17, 11632–11654. doi:10.1109/JSTARS.2024.3408154.
- Wang, D., Zhang, Q., Xu, Y., Zhang, J., Du, B., Tao, D., Zhang, L., 2022a. Advancing plain vision transformer toward remote sensing foundation model. *IEEE Transactions on Geoscience and Remote Sensing* 61, 1–15.
- Wang, Y., Albrecht, C.M., Braham, N.A.A., Mou, L., Zhu, X.X., 2022b. Self-supervised learning in remote sensing: A review. *IEEE Geoscience and Remote Sensing Magazine* 10, 213–247. doi:10.1109/MGRS.2022.3198244.
- Wang, Y., Albrecht, C.M., Zhu, X.X., 2024b. Multi-label guided soft contrastive learning for efficient Earth observation pretraining. *IEEE Transactions on Geoscience and Remote Sensing*.
- Wang, Y., Braham, N.A.A., Xiong, Z., Liu, C., Albrecht, C.M., Zhu, X.X., 2023. Ssl4eo-s12: A large-scale multimodal, multitemporal dataset for self-supervised learning in earth observation [software and data sets]. *IEEE Geoscience and Remote Sensing Magazine* 11, 98–106.
- Wang, Y., Hernández, H.H., Albrecht, C.M., Zhu, X.X., 2025. Feature guided masked autoencoder for self-supervised learning in remote sensing. *IEEE Journal of Selected Topics in Applied Earth Observations and Remote Sensing* 18, 321–336. doi:10.1109/JSTARS.2024.3493237.
- Wu, K., Zhang, Y., Ru, L., Dang, B., Lao, J., Yu, L., Luo, J., Zhu, Z., Sun, Y., Zhang, J., Zhu, Q., Wang, J., Yang, M., Chen, J., Zhang, Y., Li, Y., 2025. A semantic-enhanced multi-modal remote sensing foundation model for earth observation. *Nature Machine Intelligence* URL: <https://doi.org/10.1038/s42256-025-01078-8>, doi:10.1038/s42256-025-01078-8.
- Wu, Z., Sun, J., Zhang, Y., Zhu, Y., Li, J., Plaza, A., Benediktsson, J.A., Wei, Z., 2021. Scheduling-guided automatic processing of massive hyperspectral image classification on cloud computing architectures. *IEEE Transactions on Cybernetics* 51, 3588–3601. doi:10.1109/TCYB.2020.3026673.
- Xiao, A., Xuan, W., Wang, J., Huang, J., Tao, D., Lu, S., Yokoya, N., 2025. Foundation models for remote sensing and earth observation: A survey. *IEEE Geoscience and Remote Sensing Magazine*.
- Xiong, Z., Chen, S., Shi, Y., Zhu, X.X., 2024a. Self-supervised pretraining with monocular height estimation for semantic segmentation. *IEEE Transactions on Geoscience and Remote Sensing* 62, 1–12. doi:10.1109/TGRS.2024.3412629.
- Xiong, Z., Wang, Y., Zhang, F., Stewart, A.J., Hanna, J., Borth, D., Papoutsis, I., Saux, B.L., Camps-Valls, G., Zhu, X.X., 2024b. Neural plasticity-inspired foundation model for observing the Earth crossing modalities. *arXiv preprint arXiv:2403.15356*.
- Xu, Y., Ma, Y., Zhang, Z., 2024. Self-supervised pre-training for large-scale crop mapping using sentinel-2 time series. *ISPRS Journal of Photogrammetry and Remote Sensing* 207, 312–325.
- Yuan, Y., Lin, L., Liu, Q., Hang, R., Zhou, Z.G., 2022. Sits-former: A pre-trained spatio-spectral-temporal representation model for sentinel-2 time series classification. *International Journal of Applied Earth Observation and Geoinformation* 106, 102651.
- Zhang, L., Zhang, L., 2022. Artificial intelligence for remote sensing data analysis: A review of challenges and opportunities. *IEEE Geoscience and Remote Sensing Magazine* 10, 270–294.
- Zhang, L., Zhang, L., Du, B., 2016. Deep learning for remote sensing data: A technical tutorial on the state of the art. *IEEE Geoscience and Remote Sensing Magazine* 4, 22–40.
- Zhang, X., Yu, W., Pun, M.O., Shi, W., 2023. Cross-domain landslide mapping from large-scale remote sensing images using prototype-guided domain-aware progressive representation learning. *ISPRS Journal of Photogrammetry and Remote Sensing* 197, 1–17.
- Zhang, X., Zhou, C., Huang, J., Zhang, L., 2025. Tpv-seg: Textually enhanced prompt tuning of vision-language models for open-vocabulary remote sensing semantic segmentation. *IEEE Transactions on Geoscience and Remote Sensing* 63, 1–17. doi:10.1109/TGRS.2025.3624767.